Fast analyses and designs of long-period fiber grating devices with cosine-class apodizations by using Fourier mode coupling theory

Xiangkai Zeng[1,*] and Lai Wei[2]

[1]School of Optoelectronic Information, Chongqing University of Technology, Chongqing 400054, China

[2]Department of Electronic and Information Engineering, Hong Kong Polytechnic University, Hong Kong, China

*Corresponding author: zxkai@cqut.edu.cn

Received 14 August 2013; accepted 3 October 2013;
posted 7 October 2013 (Doc. ID 194376); published 30 October 2013

This paper presents an analytical approach to fast analyzing and designing long-period fiber grating (LPFG) devices with cosine-class apodizations by using the Fourier mode coupling (FMC) theory. The LPFG devices include LPFGs, LPFG-based in-fiber Mach–Zehnder and Michelson interferometers, which are apodized with the cosine-class windows of cosine, raised-cosine, Hamming, and Blackman. The analytic models (AMs) of the apodized LPFG devices are derived from the FMC theory, which are compared with the preferred transfer matrix (TM) method to confirm their efficiencies and accuracies. The AM-based analyses are achieved and verified to be accurate and efficient enough. The AM-based analysis efficiency is improved over 1318 times versus the TM-based one. Based on the analytic models, an analytic design algorithm is proposed and then applied to designing these LPFG devices, which has the complexity of $O(N)$ and is far faster than the existing design methods.

OCIS codes: (050.2770) Gratings; (060.2310) Fiber optics; (070.7345) Wave propagation; (230.7370) Waveguides.

http://dx.doi.org/10.1364/AO.52.007609

1. Introduction

Long-period fiber grating (LPFG) can couple its propagating core-mode to codirectional cladding modes and *vice versa*, which is very different from fiber Bragg grating (FBG). Two cascaded LPFGs construct an in-fiber Mach–Zehnder interferometer (MZI) [1,2] and one LPFG with a terminal reflector functions as an in-fiber Michelson interferometer (MI) [3,4]. Thus LPFG devices include LPFG, LPFG-based MZI, and MI. LPFGs are often used for band-rejection filters, gain equalizers, or sensors in optical sensing and communication systems [5–8]. LPFG-based MZIs and MIs are usually employed for highly sensitive measurements and multi-wavelength filters [1–4]. Uniform LPFG can be easily fabricated, whereas it has undesirable sidebands that can cause cross talk among channels in wavelength-division-multiplexing systems. The spectral response of an LPFG in applications should be shaped to reduce its sidebands. This can be implemented by apodizing its index change with Gaussian or cosine-type windows because there have been some fabrication techniques to permit the precise controls of both the local grating pitch and the apodization profile along the LPFG [9]. The functions of cosine-type windows include cosine, raised-cosine (RC), Hamming (i.e., improved RC), and Blackman (i.e., the second-order RC) etc. Cosine-class apodizations can extremely restrain the spectral sidebands of LPFGs. Like Gaussian apodization, they may possess nonuniform (NU) or uniform "DC" index changes, which can lead to distinguishable spectra. For an LPFG with NU-DC

1559-128X/13/317609-09$15.00/0

index change, there are sidebands on the short-wavelength side and no sideband on the long-wavelength side of its transmission spectrum, since the wings of the apodized LPFG act like a MZI at short wavelength and then cause the undesirable sidebands on the short-wavelength side. However for an LPFG with extremely small NU or uniform "DC" index changes, there is no sideband on the long- and short-wavelength sides. This type of apodized LPFGs is commonly used to reduce the undesirable sidebands in practice. Therefore the apodized LPFG devices of interest in this paper are confined to those with extremely small NU or uniform "DC" index perturbations.

LPFG device is without any reflection, so its most important property is transmission response that is determined by the profile of its index perturbation. Analyzing an LPFG device is to get its transmission spectrum from its index change. But designing an LPFG device is to obtain the profile of its index change from its desired transmission spectrum. Actually this is an inverse problem, which has attracted more research interest. Fast and exactly analyzing and designing LPFG devices are significant in their fabrications and applications. LPFG devices with cosine-class apodizations are nonuniform. The existing methods available to analyze the apodized LPFGs are just only numerical methods, such as the transfer matrix (TM) [10,11], Runge–Kutta algorithm, Bloch wave, and electromagnetic scattering methods [12,13], etc. The TM method, which is based on the well-known coupled-mode theory, is the most often exploited and preferred. These numerical analysis methods are time-consuming and restricted by accumulative errors. On the other hand, for solving the inverse problem, there are fewer methods for designing LPFGs because LPFG is finite-impulse-response filter, and each point in its impulse response is determined by the entire grating, which is very different from FBG. The existing algorithms for designing LPFGs mainly include the Gel'fand–Levitan–Marchenko (GLM) method [14], the layer-peeling (LP) algorithm [15,16], and the genetic algorithm (GA) [17], etc. The GLM method can give satisfying results even for strong coupling gratings. The LP method reconstructs LPFGs layer by layer in a recursive manner based on the causality rule. The GA method is to combine a genetic algorithm with one numerical analysis technique and one design method as abovementioned, where the design method is used for designing the LPFG device with target transmission, and the analysis technique is for calculating the transmission of the designed LPFG device, and the genetic algorithm is for optimizing the design by searching the type and parameter values of the designed LPFG structure, on the base of the error relation between the calculated and target transmissions. The main drawback of the GA method is its run-time, which is about 100 times that of the iterative GLM method. These design algorithms have a complexity that grows as about $O(N^2)$ [18], where N is the number of points in an LPFG. Thus they also have lower efficiencies and accumulative errors, owing to their N^2 operations.

An analytic model of LPFG can straightforwardly describe the effects of its index changes on its transmission spectrum, which can provide fast and exact calculations. Analytically modeling LPFGs may be the best way to improve the efficiency of analyzing and designing LPFGs. However, in traditional viewpoints, it is very difficult to get the analytic models of NU-LPFGs, and the analytic solutions for apodized LPFGs are nonexistent. Recently the Fourier mode coupling (FMC) theory was proposed for analyzing the spectra of NU-LPFGs [19]. The analytic solutions for some NU-LPFGs have been founded by using the FMC theory [20]. This means that some specific NU-LPFGs probably have analytic models, which may let us obtain an analytic approach to analyzing and designing the NU-LPFGs. According to the FMC theory, we here try to derive the analytic models of the transmissions of LPFG, LPFG-based MZI, and MI, which are apodized with the cosine-class windows of cosine, raised-cosine, Hamming, and Blackman and then utilize these models to fast analyze and design these apodized LPFG devices. This is an analytic technique but not a numerical method.

2. Universal Solutions for LPFG Devices

One LPFG will cause the coupling between its propagating core mode and codirectional cladding mode without any reflection, which is determined by the index perturbation in the LPFG. The mode couplings in LPFG, LPFG-based in-fiber MZI, and MI are schematically shown in Figs. 1(a), 1(b), and 1(c), respectively.

It is assumed that the index perturbation in any LPFG device is created uniformly across its core and is nonexistent outside the core. Based on the FMC theory, the coupled-mode equation for an LPFG can be written as [19]

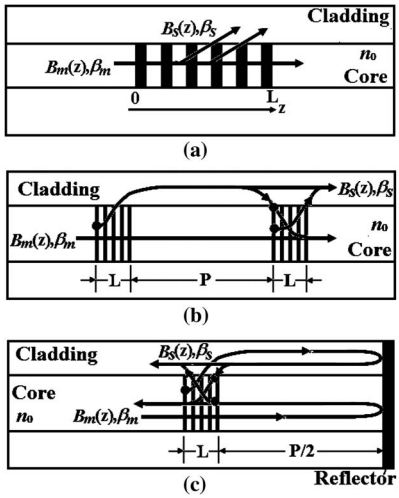

Fig. 1. Mode couplings in (a) LPFG, (b) LPFG-based MZI, and (c) LPFG-based MI.

$$\frac{dB_s(z)}{dz} = -\sum_m jkB_m(z)\Delta n(z)e^{-j(\beta_m-\beta_s)z}, \quad (1)$$

with

$$k = 0.5\varepsilon_0\omega n_0 \iint_\Omega E_m(r,\varphi)E_s^*(r,\varphi)\mathrm{d}A,$$

where z is the wave propagating direction, $\Delta n(z)$ is the profile of the index change, and m and s are the orders of the propagating core mode and the coupled cladding mode, respectively; $B_m(z)$ and $B_s(z)$ are amplitude coefficients; β_m and β_s are propagation constants; k is the coupling coefficient between the core and cladding modes, ε_0 is the permittivity of vacuum, ω is angular frequency, n_0 is the refractive index of the core, A is the cross-section area, Ω is the whole cross-section area, r and ϕ are the axes of cylindrical coordinate system, and E_m and E_s are the electric fields of the propagating core mode and the coupled cladding mode, respectively.

The boundary conditions are $B_m(0) = 1$ and $B_s(0) = 0$ for LPFGs. In the case of two-mode coupling, the integration of Eq. (1) is performed along the z axis within the limits of the start and end positions of the LPFG, which directly leads to

$$\int_0^{B_s(L)} \frac{dB_s(z)}{B_m(z)} = -jk\int_0^L \Delta n(z)e^{-j(\beta_m-\beta_s)z}\mathrm{d}z, \quad (2)$$

where L is the length of the LPFG, $\beta_m = 2\pi(n_m + \delta_{n0})/\lambda$ and $\beta_s = 2\pi n_s/\lambda$, where δ_{n0} is the effective-index change caused by the index change, λ is the wavelength in vacuum, and n_m and n_s are the effective indices of the propagating core mode and the coupled cladding mode, respectively. The Fourier transform (FT) of the index change $\Delta n(z)$ in the LPFG is defined as

$$\int_0^L \Delta n(z)e^{-j2\pi v_L z}\mathrm{d}z = M(v_L)e^{j\phi(v_L)}, \quad (3)$$

where $\nu_L = (n_m + \delta_{n0} - n_s)/\lambda$, $M(v_L)$, and $\varphi(v_L)$ are the modulus and phase, respectively, of the FT result. According to the law of conservation of flux [21], the relation between the amplitude coefficients $B_m(z)$ and $B_s(z)$ is governed by

$$B_m^2(z) = B_m^2(0) - B_s^2(z). \quad (4)$$

By substituting Eqs. (3) and (4) into Eq. (2), we are able to solve Eq. (2) for $B_m(z)$ and $B_s(z)$ in the case of phase matching and then obtain the power transmission $T = 1 - |B_s(L)|^2/|B_m(0)|^2$ of the LPFG, given by

$$T = \cos^2[kM(\nu_L)]. \quad (5)$$

Equation (5) is a universal solution to the power transmission of any LPFG, which is also fit for LPFG-based in-fiber MZI and MI. When modeling LPFG-based MZI and MI, we just take any LPFG-based interferometer to be a wholly single NU-LPFG, and then derive the analytic model of the NU-LPFG from the FMC theory. The analytic model of the NU-LPFG is regarded as that of the LPFG-based interferometer. For LPFG-based MZI, its two cascaded LPFGs are usually identical, thus its index change $\Delta n_M(z)$ can be described by $\Delta n_M(z) = \Delta n(z) + \Delta n(z - P - L)$, where P is the interval between the two LPFGs. LPFG-based MI can be also described by the same expression as the MZI, only if P in the MI equals two times the space between its LPFG and terminal reflector without attenuation. By using $\Delta n_M(z)$ instead of $\Delta n(z)$ in Eq. (3), the modulus $M_I(\nu_L)$ of the FT result of the index changes $\Delta n_M(z)$ can be obtained, as $M_I(\nu_L) = 2M(\nu_L)\cos[\pi\nu_L(P + L)]$. Incorporating $M_I(\nu_L)$ into Eq. (5) can yield the power transmission T_M of the in-fiber MZI or MI, described by

$$T_M = \cos^2\{2kM(v_L)\cos[\pi v_L(P + L)]\}. \quad (6)$$

Various LPFG devices are with different perturbations, which lead to the changes of their FTs, then result in a variety of power transmissions. Once the profile of the index change in an LPFG device is determined, its transmission spectrum can be analyzed according to above equations. Hence the transmission spectra of the LPFG devices with cosine-class apodizations can be possibly modeled on Eqs. (3), (5), and (6).

3. Fast Analyses of the Apodized LPFG Devices

A. Analytic Models

For an apodized LPFG with uniform or extremely small NU "DC" index changes, its index change $\Delta n(z)$ can be generally modeled as

$$\Delta n(z) = \delta_n[1 - w(z)V\cos(2\pi z/\Lambda)], \quad (7)$$

where $z \in [0, L]$, $w(z)$ is the window function of apodization, V is the fringe visibility of the index change, Λ is nominal period, and δ_n is the "DC" index change spatially averaged over a grating period. For the index perturbation with NU-DC index change, it can be expressed as $\Delta n(z) = \delta_n w(z)(1 - V\cos(2\pi z/\Lambda)$, which has undesirable sidebands on the short-wavelength side. Therefore here we deal with only the apodized LPFGs described by Eq. (7). The profiles of the index changes in the LPFGs are apodized with the cosine-class windows of cosine, raised-cosine, Hamming, and Blackman. The window functions in the cosine-apodized (CA), raised-cosine-apodized (RCA), Hamming-apodized (HA), and Blackman-apodized (BA) LPFGs are shown in Fig. 2.

Hereinafter, the subscripts c, r, H, and B denote the windows of cosine, raised-cosine, Hamming, and Blackman, respectively, and the subscripts Mc, Mr, MH, and MB denote the LPFG-based in-fiber

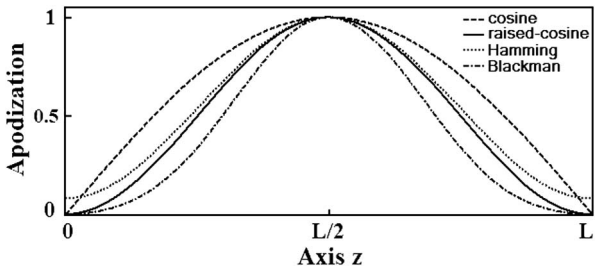

Fig. 2. Window functions of the apodizations in cosine-, raised-cosine-, Hamming-, and Blackman-apodized LPFG devices.

interferometers formed by CA-, RCA-, HA-, and BA-LPFGs, respectively. The window functions of the apodizations in CA-, RCA-, HA-, and BA-LPFGs can be written as Eqs. (8), (9), (10), and (11), respectively:

$$w_c(z) = \cos[\pi(L-2z)/(2L)], \tag{8}$$

$$w_r(z) = 0.5 + 0.5\cos[\pi(L-2z)/L], \tag{9}$$

$$w_H(z) = 0.54 + 0.46\cos[\pi(L-2z)/L], \tag{10}$$

$$w_B(z) = 0.42 + 0.5\cos[\pi(L-2z)/L] + 0.08\cos[2\pi(L-2z)/L]. \tag{11}$$

By incorporating Eq. (3) with Eqs. (8), (9), (10), and (11), we can derive the moduli M of the FT results of the index changes in the CA-, RCA-, HA-, and BA-LPFGs, given by Eqs. (12), (13), (14), and (15), respectively

$$M_c = \frac{\delta_n LV\cos(\pi L\sigma_L)}{2\pi(1-4L^2\sigma_L^2)}, \tag{12}$$

$$M_r = \frac{\delta_n LV\,\mathrm{sinc}(\pi L\sigma_L)}{8(1-L^2\sigma_L^2)}, \tag{13}$$

$$M_H = \left(\frac{0.135-0.02L^2\sigma_L^2}{1-L^2\sigma_L^2}\right)\delta_n LV\,\mathrm{sinc}(\pi L\sigma_L), \tag{14}$$

$$M_B = \left(\frac{0.42-0.045L^2\sigma_L^2}{4-5L^2\sigma_L^2+L^4\sigma_L^4}\right)\delta_n LV\,\mathrm{sinc}(\pi L\sigma_L), \tag{15}$$

where $\mathrm{sinc}(x) = \sin(x)/x$, $\sigma_L = v_L - 1/\Lambda$ is the detuning parameter for codirectional coupling. Then substituting Eqs. (12), (13), (14), or (15) into Eq. (5), we are able to mathematically calculate the power transmissions of the CA-, RCA-, HA-, or BA-LPFGs, determined by Eqs. (16), (17), (18), or (19), respectively:

$$T_c = \cos^2\left[\frac{k\delta_n LV\cos(\pi L\sigma_L)}{2\pi(1-4L^2\sigma_L^2)}\right], \tag{16}$$

$$T_r = \cos^2\left[\frac{k\delta_n LV\,\mathrm{sinc}(\pi L\sigma_L)}{8(1-L^2\sigma_L^2)}\right], \tag{17}$$

$$T_H = \cos^2[k\delta_n LV\,\mathrm{sinc}(\pi L\sigma_L) \times (0.135-0.02L^2\sigma_L^2)/(1-L^2\sigma_L^2)], \tag{18}$$

$$T_B = \cos^2[k\delta_n LV\,\mathrm{sinc}(\pi L\sigma_L) \times (0.42-0.045L^2\sigma_L^2)/(4-5L^2\sigma_L^2+L^4\sigma_L^4)]. \tag{19}$$

By similarly substituting Eqs. (12), (13), (14), or (15) into Eq. (6), we can also obtain the power transmissions of the CA-, RCA-, HA-, or BA-LPFG-based MZI/MIs, described by Eqs. (20), (21), (22), or (23), respectively:

$$T_{\mathrm{Mc}} = \cos^2\left\{\frac{k\delta_n LV\cos[\pi v_L(P+L)]\cos(\pi L\sigma_L)}{\pi(1-4L^2\sigma_L^2)}\right\}, \tag{20}$$

$$T_{\mathrm{Mr}} = \cos^2\left\{\frac{k\delta_n LV\cos[\pi v_L(P+L)]\mathrm{sinc}(\pi L\sigma_L)}{4(1-L^2\sigma_L^2)}\right\}, \tag{21}$$

$$T_{\mathrm{MH}} = \cos^2\{k\delta_n LV\cos[\pi v_L(P+L)]\mathrm{sinc}(\pi L\sigma_L) \times (0.27-0.04L^2\sigma_L^2)/(1-L^2\sigma_L^2)\}, \tag{22}$$

$$T_{\mathrm{MB}} = \cos^2\{k\delta_n LV\cos[\pi v_L(P+L)]\mathrm{sinc}(\pi L\sigma_L) \times (0.84-0.09L^2\sigma_L^2)/(4-5L^2\sigma_L^2+L^4\sigma_L^4)\}. \tag{23}$$

Equations (16), (17), (18), and (19) are the analytic models of the power transmissions of the CA-, RCA-, HA-, and BA-LPFGs, respectively, and Eqs. (20), (21), (22), and (23) are those of the CA-, RCA-, HA-, and BA-LPFG-based interferometers, respectively. The interferometers include in-fiber MZIs and MIs, in which the LPFGs are apodized with cosine-class windows. These analytic models can be exploited for fast analyzing and designing the apodized LPFG devices.

B. AM-Based Analyses

To verify the accuracy and efficiency of the above analytic models, they are applied to calculating the transmission spectra of the LPFG devices with cosine-class apodizations and are compared to the TM method [10], since the TM method is still preferred and prior to other numerical analysis methods in precision and efficiency.

Suppose that the given LPFGs with quasi-sinusoidal index changes are inscribed in single-mode (SM) fibers with the effective index $n_m = 1.462$ of core mode LP_{01}. The LPFGs couple the core mode LP_{01} to one codirectional cladding mode with the effective index $n_s = 1.4585$, which are apodized with the window functions of cosine, raised-cosine, Hamming, or Blackman. These apodized LPFGs have identical structural parameters with the exception of apodization windows, described by grating length $L = 60$ mm, period $\Lambda = 400$ μm, "DC" index change $\delta_n = 4 \times 10^{-4}$, fringe visibility $V = 1$, normalized $k = 115.7\ \pi$N/s, and the effective-index change $\delta_{n0} \approx \delta_n$ of the core mode. In the TM method, one NU-LPFG is divided into 100 piecewise-uniform segments. Figures 3(a), 3(b), 3(c), and 3(d) illustrate the calculated transmissions of the CA-, RCA-, HA-, and BA-LPFGs, respectively, which are based on the TM method (dotted lines) and the analytic models [i.e., Eqs. (16)–(19)] (solid lines), in the case of varying grating length and "DC" index change. In Fig. 3, the lines labeled 1 represent the cases with $L = 60$ mm and $\delta_n = 4 \times 10^{-4}$, and the lines labeled 2 represent the cases of $L = 30$ mm and $\delta_n = 4 \times 10^{-4}$, and the lines labeled 3 represent the cases with $L = 40$ mm and $\delta_n = 3.2 \times 10^{-4}$. The calculated spectra in Fig. 3 indicate that the cosine-class apodizations can restrain the spectral sidebands of LPFGs and that the apodized LPFGs have different performances even if they have identical structural parameters. The RCA-, HA-, and BA-LPFGs are without any sideband, while the BA-LPFG has a broader and smaller rejection band than the CA-, RCA-, and HA-LPFGs. The CA-LPFG is with some little sidebands, whereas it has narrower and larger rejection band than the RCA-, HA-, and BA-LPFGs.

Two identical LPFGs are written into a length of the same SM fiber as the above mentioned, which construct an in-fiber MZI. The LPFGs are apodized with the window functions of cosine, raised-cosine, Hamming, or Blackman. The MZI is determined by the parameters as $\Lambda = 400$ μm, $L = 30$ mm, $\delta_n = 4 \times 10^{-4}$, interval $P = 14$ cm, and normalized $k = 115.7\ \pi$N/s. Figures 4(a), 4(b), 4(c), and 4(d) exhibit the power transmissions of the in-fiber MZIs formed by the CA-, RCA-, HA-, and BA-LPFGs, respectively, which are calculated from the TM method (dotted lines) and the analytic models [i.e., Eqs. (20)–(23)] (solid lines). When the space between the LPFG and the terminal reflector in LPFG-based MIs equals 7 cm, the transmission spectra of the CA-, RCA-, HA-, and BA-LPFG-based MIs are the same as the CA-, RCA-, HA-, and BA-LPFG-based MZIs, correspondingly.

C. Accuracy and Efficiency of AM-Based Analyses

The transmission spectra shown in Figs. 3 and 4 illustrate that the AM-based transmissions of the apodized LPFG devices are in excellent agreement with the TM-based ones, in aspects of profile, pit, resonant wavelength, rejection band, and sidebands, etc. This has confirmed that the analytic models are

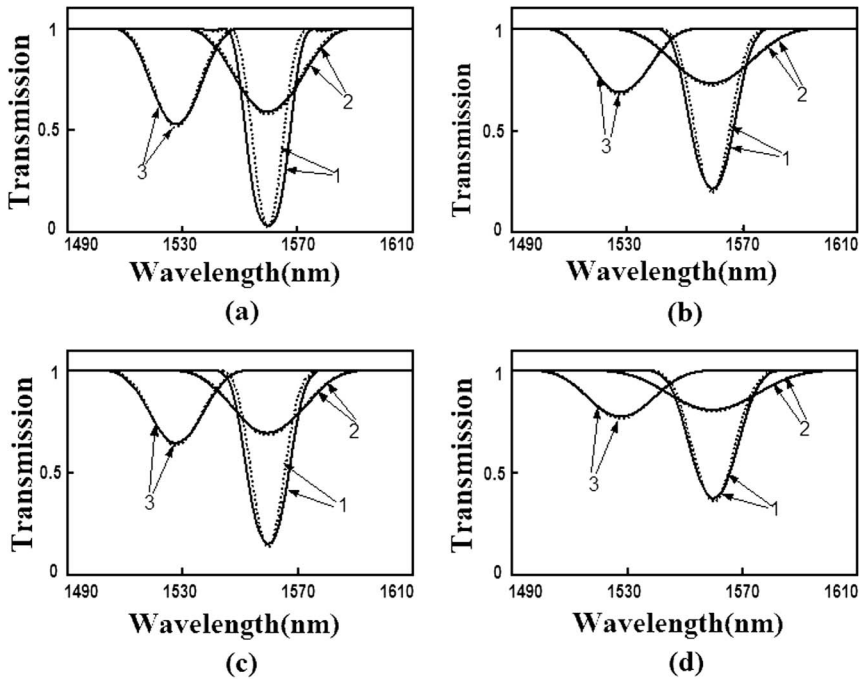

Fig. 3. Calculated transmissions of the (a) CA-; (b) RCA-; (c) HA-; and (d) BA-LPFGs along with varying their "DC" index changes and lengths by using the analytic models (solid lines) and the TM method (dotted lines).

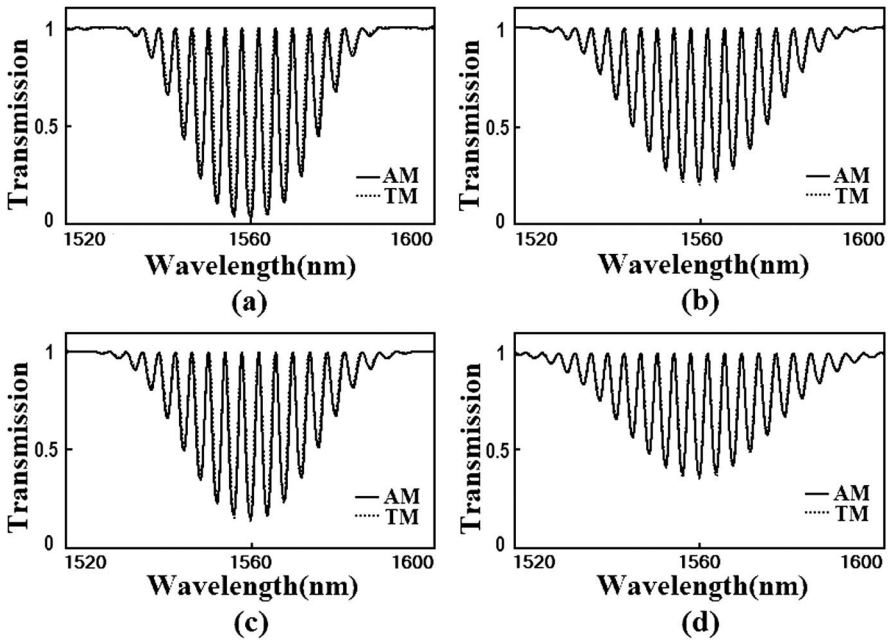

Fig. 4. Calculated transmissions of the (a) CA-; (b) RCA-; (c) HA-; and (d) BA-LPFG-based MZIs, according to the analytic models (solid lines) and the TM method (dotted lines).

accurate enough for analyzing the CA-, RCA-, HA-, and BA-LPFG devices that include LPFGs, LPFG-based MZIs, and MIs. In respect of efficiency, all the above calculations were achieved on a PC as Founder S360R with the Vista OS and Matlab5.3. In the cases of 20 pm wavelength resolution, 200 nm span, and 100 segment division in each LPFG, the TM method needs the average duration of 30.908 s at least for analyzing the CA-, RCA-, HA-, or BA-LPFGs and needs 31.116 s at least for the CA-, RCA-, HA-, or BA-LPFG-based MZIs. However, the analytic models require the average duration of 19.23 ms at most for analyzing the CA-, RCA-, HA-, or BA-LPFGs, and require 23.6 ms at most for the CA-, RCA-, HA-, or BA-LPFG-based MZIs. These durations imply that the AM-based efficiencies are increased over 1607 and 1318 times versus the TM-based ones for analyzing the apodized LPFGs and the apodized-LPFG-based MZI/MIs, respectively. Therefore the analytic models are highly efficient and accurate enough for analyzing the LPFG devices with the cosine-class apodizations.

4. Fast Designs of the Apodized LPFG Devices

A. AM-Based Design Algorithm

The index change in an apodized LPFG can be described by a specific function with some structural parameters, such as grating length, period, window type, and amplitude etc. At the same time, the transmission spectrum of an apodized LPFG can be determined by some key spectrum specifications, such as resonant wavelength λ_0, minimum transmission T_0, or maximum loss $1 - T_0$, rejection bandwidth W and the pitch Δ of interference fringe in MZI/MIs, etc. As aforementioned, designing an apodized LPFG is thus just to calculate its structural parameters from its desired transmission specifications. The above analytic models have indicated the relations of the transmissions with the structural parameters, which imply that the relations of the structural parameters with the spectral specifications may be derived from the analytic models. These relations can be directly employed to design the apodized LPFG devices. Looking at the excursion of σ_L from $\sigma_L = 0$ that causes the transmission expressions in Eqs. (16)–(19) to go to minimum, we find the resonant wavelength $\lambda_0 = (n_m + \delta_{n0} - n_s)\Lambda$ for an LPFG with a variety of the cosine-class apodizations. This is accordant with the coupled-mode theory. In the case of $\lambda = \lambda_0$, Eqs. (16), (17), (18), and (19) predict the minimum transmissions T_0 of the CA-, RCA-, HA-, and BA-LPFG devices, respectively, expressed by

$$T_0 = \cos^2(\zeta k \delta_n L V), \tag{24}$$

where $\zeta = 0.5/\pi$, 0.125, 0.135, and 0.105 for CA-, RCA-, HA-, and BA-LPFGs, respectively, and $\zeta = 1/\pi$, 0.25, 0.27, and 0.21 for CA-, RCA-, HA-, and BA-LPFG-based MZIs, respectively. The measurable bandwidth W of an LPFG is the width of the main rejection band in its transmission spectrum, which is determined by the difference between the first 1-transmission wavelengths on either side of the maximum loss. An LPFG-based MZI is with the same bandwidth as one LPFG in the MZI. According to the analytic models, the CA-, RCA-, HA-, and BA-LPFGs will be with lossless transmissions when at least $L\sigma_L = \pm 1.5$, $L\sigma_L = \pm 2$, $L\sigma_L = \pm 2$, and $L\sigma_L = \pm 3$, respectively. Then we find the rejection bandwidths W of the CA-, RCA-, HA-, and BA-LPFG devices, given by

$$W = \eta\lambda_0\Lambda/L, \tag{25}$$

where $\eta = 3$, 4, 4, and 6 for CA-, RCA-, HA-, and BA-LPFG devices, respectively. The HA-LPFG device has the same bandwidth expression as RCA-LPFG device. The fringe pitch Δ in the transmission spectra of CA-, RCA-, HA-, and BA-LPFG-based MZI/MIs can be easily derived from Eqs. (20)–(23), such that

$$\Delta = \lambda_0\Lambda/(P + L + \Lambda). \tag{26}$$

Equations (24)–(26), which are the relations of the main spectrum specifications with structural parameters, can be used to design the LPFG devices with the cosine-class apodizations. They can allow us to directly get the structural parameters of the designed LPFG devices with desired transmission specifications. Given the expected spectrum specifications as λ_0, W, T_0, and Δ, an analytic algorithm for designing the apodized-LPFG devices can be proposed according to the above relations, which is described as the following:

At step 1, choose a fiber, an apodization window and visibility V, then calculate the effective indices (n_m, n_s) of the core mode and the coupled cladding mode from the dispersion relation;
At step 2, let $\delta_{n0} = 0$, and calculate k by using n_0 and λ_0;
At step 3, calculate period $\Lambda = \lambda_0/(n_m + \delta_{n0} - n_s)$ with n_m, n_s, δ_{n0} and λ_0;
At step 4, calculate length $L = \eta\lambda_0\Lambda/W$ from Eq. (25);
At step 5, calculate $\delta_n = a\cos[(T_0)^{0.5}]/(\zeta kLV)$ from Eq. (24);
At step 6, let $\delta_{n0} \approx \delta_n$;
At step 7, if $(n_m + \delta_{n0} - n_s)\Lambda \neq \lambda_0$, go to Step 3; else, go to Step 8;
At step 8, calculate $\Delta n(z)$ from Eqs. (7) and (8); for designing LPFG-based MZI/MIs, calculate $P = (\lambda_0/\Delta - 1)\Lambda - L$ with Eq. (26), then calculate $\Delta n_M(z) = \Delta n(z) + \Delta n(z - P - L)$.

The structural parameters of an LPFG device contain fiber structure, apodization window, period, length, "DC" and "AC" index changes, etc. The calculated $\Delta n(z)$ and $\Delta n_M(z)$ represent the profiles of the index changes in the designed LPFG and MZI/MI, respectively, which have fully described the structures of the designed LPFG devices with the expected transmission spectra. So far, the analytic algorithm for designing the LPFG devices with cosine-class apodizations has been presented. Its complexity just grows as $O(N)$, which means that it needs extremely fewer operations than the existing methods with the complexity of commonly $O(N^2)$.

B. Examples of AM-Based Designs

According to the analytic algorithm proposed, we now design the apodized LPFGs with the expected transmission specifications as central wavelength $\lambda_0 = 1550$ nm, pit transmission $T_0 = 0.02$, rejection bandwidth $W = 20$ nm. At first, we choose Corning fiber SMF-28, as an example of optical fibers, with the core diameter of 8.3 μm, the core index of 1.4681, and the cladding index of 1.4628. Second, we calculate the effective index $n_m = 1.46524$ of the core mode HE_{11}, and the effective index $n_s = 1.46162$ of one cladding mode HE_{12} by using the dispersion relation of SM fiber, and then get the normalized coupling coefficient $k = 115.68\ \pi$N/s at 1550 nm. Third, by letting $V = 0.5$ and utilizing the analytic design algorithm, we compute the values of the structural parameters: $\Lambda_c = 369.4707$ μm, $L_c = 85.902$ mm, and $\delta_{nc} = 5.7519 \times 10^{-4}$ for the designed CA-LPFG; $\Lambda_r = 372.1168$ μm, $L_r = 115.36$ mm, and $\delta_{nr} = 5.4536 \times 10^{-4}$ for the designed RCA-LPFG; $\Lambda_H = 376.2693$ μm, $L_H = 116.64$ mm, and $\delta_{nH} = 4.9939 \times 10^{-4}$ for the designed HA-LPFG; $\Lambda_B = 383.6846$ μm, $L_B = 178.41$ mm, and $\delta_{nB} = 4.1978 \times 10^{-4}$ for the designed BA-LPFG. In practice, the exactly computed values of the structural parameters, such as period, length, and interval, etc., must be rounded in order to conveniently implement the fabrications of the designed structures. Finally, we are able to calculate the index changes of the designed LPFGs by use of the computed structure parameters. Figure 5 schematically exhibits the

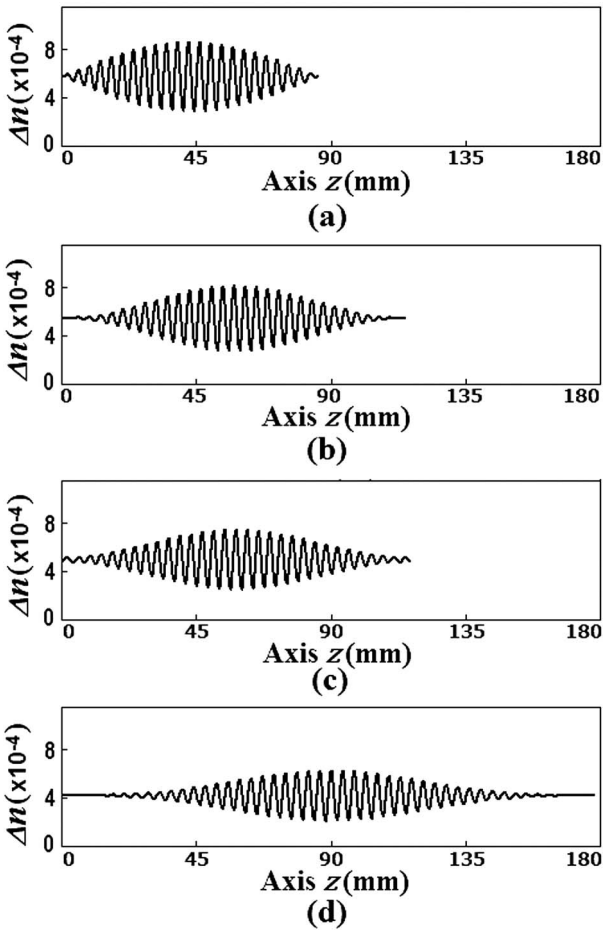

Fig. 5. Profiles of the index changes in the designed (a) CA-; (b) RCA-; (c) HA-; and (d) BA-LPFGs with the desired transmission specifications.

profiles of the index changes in the designed (a) CA-LPFG, (b) RCA-LPFG, (c) HA-LPFG, and (d) BA-LPFG, where the periods are scaled by 10 times to more clearly plot the index changes. To verify the accuracy of the resulting designs, the transmission spectra of the designed apodized-LPFGs are analyzed with the preferred TM method, which are shown in Fig. 6 in linear scale.

Like the analogous LPFGs, the apodized-LPFG-based MZIs and MIs can be also designed. It is assumed that an expected MZI, as an example of the LPFG-based interferometers, has the transmission specifications: central wavelength $\lambda_0 = 1560$ nm, minimum transmission $T_0 = 0.1$, bandwidth $W = 25$ nm, and fringe pitch $\Delta = 3$ nm. We still take the SMF-28 as the optical fiber in which the MZI is constructed. The two apodized LPFGs in the MZI are identical. Letting visibility $V = 0.5$ and using the design algorithm, we have also calculated the values of the structural parameters: $\Lambda_c = 398.8662$ μm, $L_c = 74.668$ mm, $\delta_{nc} = 2.9109 \times 10^{-4}$ and $P_c = 132.34$ mm for the designed CA-LPFG-based MZI; $\Lambda_r = 400.3118$ μm, $L_r = 99.918$ mm, $\delta_{nr} = 2.7696 \times 10^{-4}$, and $P_r = 107.84$ mm for the designed RCA-LPFG-based MZI; $\Lambda_H = 402.5804$ μm, $L_H = 100.48$ mm, $\delta_{nH} = 2.55 \times 10^{-4}$, and $P_H = 108.46$ mm for the designed HA-LPFG-based MZI; $\Lambda_B = 406.6319$ μm, $L_B = 152.24$ mm, $\delta_{nB} = 2.164 \times 10^{-4}$, and $P_B = 58.799$ mm for the designed BA-LPFG-based MZI. These computed values must be also rounded in practice. After obtaining these structural parameters, we can calculate the index changes of the designed MZIs. Figures 7(a), 7(b), 7(c), and 7(d) plot the profiles of the index changes in the designed CA-, RCA-, HA-, and BA-LPFG-based MZIs, respectively, where the periods are scaled by 15 times. To confirm the accuracy of the resulting designs, the transmission spectra of these designed MZIs are also calculated and shown in Fig. 8.

C. Accuracy and Efficiency of AM-Based Designs

Figure 6 shows that the designed LPFGs are with the central wavelength of 1550 nm, the pit transmission

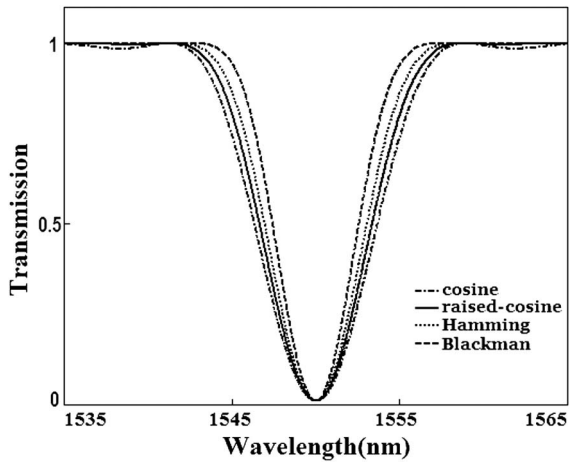

Fig. 6. Verified transmissions of the designed CA-, RCA-, HA-, and BA-LPFGs by using the TM method.

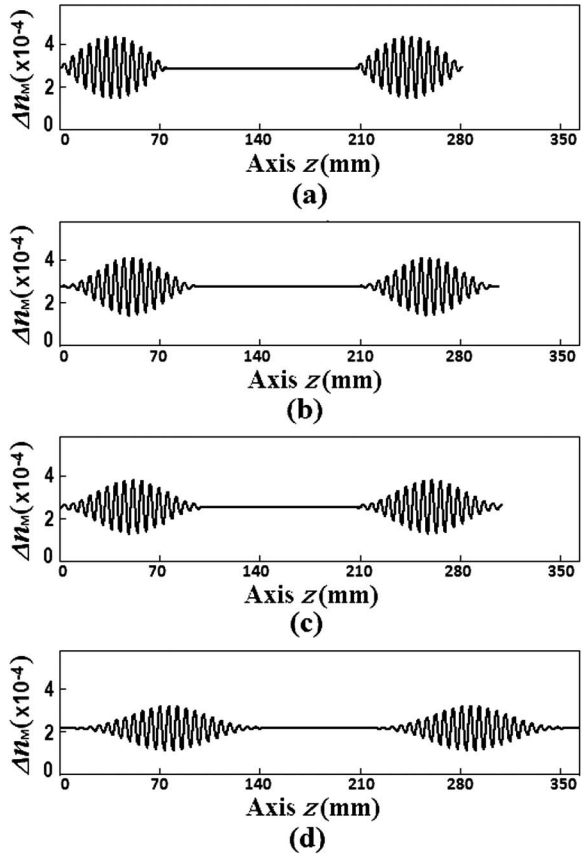

Fig. 7. Profiles of the index changes in the designed (a) CA-, (b) RCA-, (c) HA-, and (d) BA-LPFG-based MZIs with the expected transmission specifications.

of 0.02, and the rejection bandwidth of ~20 nm. Figure 8 indicates that the LPFG-based MZIs have a central wavelength of 1560 nm, a bandwidth of ~25 nm, a minimum transmission of 0.1, and a fringe pitch of 3 nm. These transmission specifications of the designed LPFG devices are in good agreement with the desired specifications, which means that the designed LPFG devices based on the analytic algorithm have the expected transmission specifications such as maximum loss, bandwidth, central wavelength, and the pitch of interference fringes. This has confirmed that the proposed design

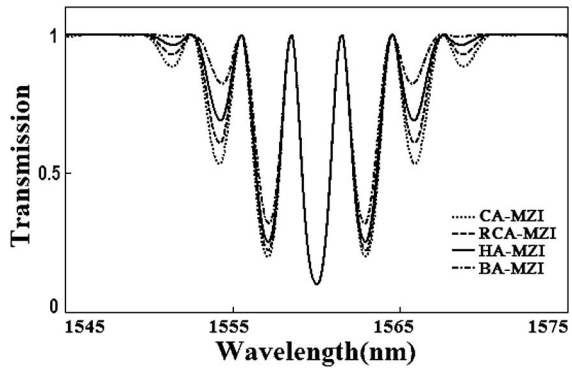

Fig. 8. Transmissions of the designed CA-, RCA-, HA-, and BA-LPFG-based MZIs.

algorithm is accurate enough. Figures 6 and 8 also demonstrate that the apodized LPFG devices will require different index changes if they have identical transmission specifications. This shows that the lengths and periods of the designed LPFG devices progressively increase, and the "DC" index changes and intervals successively decrease, in the order of CA-, RCA-, HA-, and BA-LPFG devices.

The processes of designing the above LPFG devices were achieved in the aforementioned PC system. The average time of calculating all the structural parameters is about 253 μs. In the case of 20 μm position resolution, the analytic design algorithm needs the average duration of 2.857 ms at most for designing the CA-, RCA-, HA-, or BA-LPFGs and requires 3.407 ms at most for designing the CA-, RCA-, HA-, or BA-LPFG-based MZIs. However, the existing design methods usually need the run-time of over 1 min. Therefore the analytic design algorithm proposed has much higher efficiency than the existing design methods.

5. Conclusions

This paper has presented the analytic approach to fast analyzing and designing LPFG devices with cosine-class apodizations. The LPFG devices include CA-, RCA-, HA-, and BA-LPFGs, and CA-, RCA-, HA-, and BA-LPFG-based MZI/MIs, whose sidebands are extremely restrained. The analytic models of the apodized LPFG devices are derived from the FMC theory and then are employed for designing these devices. The AM-based calculations have been achieved and compared to the TM-based ones, which have confirmed that the AM-based analyses are with enough accuracy and high efficiency being over 1318 times the TM-based efficiency.

The relations of the transmission specifications with the structural parameters are obtained from the analytic models, on which the analytic algorithm for designing these apodized LPFG devices is then proposed. Designing one of these LPFG devices is completely done in about several milliseconds by using the analytic algorithm that has the complexity of $O(N)$ and is far faster than the existing design methods. The power transmissions of the designed LPFG devices are calculated and then are verified to be with the desired transmission specifications. All the above demonstrations have illustrated that the analytic approach proposed is adaptable to fast and exactly analyzing and designing the LPFG devices with cosine-class apodizations, which has overturned the conventional viewpoint that is the absence of the analytic technique for analyzing or designing apodized LPFGs.

References

1. X. J. Gu, "Wavelength-division multiplexing isolation fiber filter and light source using cascaded long-period grating," Opt. Lett. **23**, 509–510 (1998).
2. A. P. Zhang, Z. Guan, and S. He, "Optical low-coherence reflectometry based on long-period grating Mach–Zehnder interferometer," Appl. Opt. **45**, 5733–5739 (2006).
3. P. L. Swart, "Long-period grating Michelson refractometric sensor," Meas. Sci. Technol. **15**, 1576–1580 (2004).
4. D. W. Kim, Y. Zhang, K. L. Cooper, and A. Wang, "In-fiber reflection mode interferometer based on a long-period grating for external refractive-index measurement," Appl. Opt. **44**, 5368–5373 (2005).
5. A. M. Vengsarkar, P. J. Lemaire, J. B. Judkins, V. Bhatia, T. Erdogan, and J. E. Sipe, "Long-period fiber gratings as band-rejection filters," J. Lightwave Technol. **14**, 58–65 (1996).
6. A. M. Vengsarkar, J. R. Pedrazzani, J. B. Judkins, P. J. Lemaire, N. S. Bergano, and C. R. Davidson, "Long-period fiber-grating-based gain equalizers," Opt. Lett. **21**, 336–338 (1996).
7. A. Cusano, A. Iadicicco, P. Pilla, L. Contessa, S. Campopiano, A. Cutolo, and M. Giordano, "Mode transition in high refractive index coated long period grating," Opt. Express **14**, 19–34 (2006).
8. S. M. Tripathi, W. J. Bock, A. Kumar, and P. Mikulic, "Temperature insensitive high-precision refractive-index sensor using two concatenated dual-resonance long-period gratings," Opt. Lett. **38**, 1666–1668 (2013).
9. T. Allsop, K. Kalli, K. M. Zhou, G. N. Smith, M. Komodromos, J. Petrovic, D. J. Webb, and I. Bennion, "Spectral characteristics and thermal evolution of long-period gratings in photonic crystal fibers fabricated with a near-IR radiation femtosecond laser using point-by-point inscription," J. Opt. Soc. Am. B **28**, 2105–2114 (2011).
10. T. Erdogan, "Fiber grating spectra," J. Lightwave Technol. **15**, 1277–1294 (1997).
11. F. Abrishamian and K. Morishita, "Transfer-matrix method based on a discrete coupling model for analyzing uniform and nonuniform codirectional fiber grating couplers," Appl. Opt. **51**, 2367–2372 (2012).
12. E. Peral and J. Capmany, "Generalized Bloch wave analysis for fiber and waveguide gratings," J. Lightwave Technol. **15**, 1295–1302 (1997).
13. A. Bouzid and M. A. G. Abushagur, "Scattering analysis of slanted fiber gratings," Appl. Opt. **36**, 558–562 (1997).
14. E. Peral, J. Capmany, and J. Marti, "Iterative solution to the Gel'Fand–Levitan–Marchenko coupled equations and application to synthesis of fiber gratings," IEEE J. Quant. Electron. **32**, 2078–2084 (1996).
15. R. Feced, M. N. Zervas, and M. A. Muriel, "An efficient inverse scattering algorithm for the design of nonuniform fiber Bragg gratings," IEEE J. Quantum Electron. **35**, 1105–1115 (1999).
16. L. Wang and T. Erdogan, "Layer peeling algorithm for reconstruction of long-period fibre gratings," Electron. Lett. **37**, 154–156 (2001).
17. G. Chern and L. A. Wang, "Design of binary long-period fiber grating filters by the inverse-scattering method with genetic algorithm optimization," J. Opt. Soc. Am. A **19**, 772–780 (2002).
18. A. Buryak, J. Bland-Hawthorn, and V. Steblina, "Comparison of inverse scattering algorithms for designing ultra-broadband fiber Bragg gratings," Opt. Express **17**, 1995–2004 (2009).
19. X. K. Zeng and Y. J. Rao, "Theory of Fourier mode coupling for long-period fiber gratings," Acta Phys. Sin. **59**, 8607–8614 (2010) (in Chinese).
20. X. K. Zeng and K. Liang, "Analytic solutions for spectral properties of superstructure, Gaussian-apodized and phase shift gratings with short- or long-period," Opt. Express **19**, 22797–22808 (2011).
21. J. A. Armstrong, N. Bloembergen, J. Ducuing, and P. S. Pershan, "Interactions between light waves in a nonlinear dielectric," Phys. Rev. **127**, 1918–1939 (1962).